

Continuous-wave cavity-enhanced polarimetry for optical rotation measurement of chiral molecules

Dang-Bao-An Tran^{*}, Katherine M. Manfred, Robert Peverall, Grant A. D. Ritchie^{*}

Department of Chemistry, Physical and Theoretical Chemistry Laboratory, University of Oxford, South Parks Road, Oxford, OX1 3QZ, United Kingdom

ABSTRACT: Precise optical rotation measurements plays an important role in the analysis of chiral molecules in various fields, especially in biological chemistry and pharmacology. In this paper, we demonstrate a new variant of continuous-wave cavity enhanced polarimetry for detecting the optical activity of two enantiomers of a chiral molecule at 730 nm. It is based on a signal reversing technique for which the chiral specific rotation is directly determined by the cavity ring-down signal from two counter-propagating beams in a bow-tie cavity. In particular, we ensure reproducible excitation of both modes by broadening the linewidth of the diode laser source by application of a radiofrequency perturbation to its injection current. The performance of the polarimeter is demonstrated for the specific rotation of (+)- and (–)- α -pinene in different environments, including the pure vapour, open air, and the liquid phase; the detection precision ranges between 10^{-5} and 10^{-4} degrees per cavity pass depending on the environment. The apparatus is a robust and practical tool for quantifying chirality and can be developed for the entire visible and near-infrared spectral regions.

Chirality is ubiquitous in many areas of science, and chiral molecules play an important role in many aspects of biological life, the pharmaceutical industry, and in testing fundamental physics. Indeed, one of the greatest mysteries in the evolution of life on Earth is the origin of biomolecular homochirality – the preference for organisms to almost exclusively use right-handed sugars and left-handed amino acids over their enantiomers¹. While enantiomers of a chiral molecule ostensibly exhibit identical chemical properties, they can exhibit different toxicity to cells, and thus detecting and quantifying enantiometric excess (*ee*) has an essential role in drug development². In physics, the breaking of mirror image symmetry (parity violation) is considered of fundamental importance^{3,4} and chiral molecules have been identified as relevant candidates for studying parity-violation inherent in the weak nuclear force as described by the standard model^{5,6}.

In recent years, a range of sophisticated optical techniques has been developed to determine chirality including microwave spectroscopy^{7,8}, femtosecond excitation⁹, superchiral light¹⁰, circular-differential luminescence spectroscopy¹¹, and ionization imaging¹². The predominant methods for directly measuring chirality however remain electronic circular dichroism (ECD), vibrational circular dichroism (VCD) and optical rotation, relying on the interaction of polarized light with chiral samples^{13–15}. The latter can be measured far from molecular absorption features while the circular dichroism techniques are performed on resonance. Moreover, the chiral signals in the mid-IR domain, which hosts the vibrational modes of chiral molecules, are typically small in comparison with the background signals caused by the presence of linear birefringence due to strain in optical components. In addition, less sensitive detection and higher

levels of background noise in this spectral region create requirements for higher sample density and longer averaging times¹⁶. Modern commercial polarimeters have typical precision of ~ 1 millidegree, mainly limited by spurious backgrounds caused by the effect of birefringence. A variety of different pulsed cavity ring-down polarimetry (CRDP) arrangements have been demonstrated in order to enhance the detection of chirality by providing an extended optical path length over which the polarised radiation can interact with the chiral sample. Importantly, it should be noted that while a high-finesse linear cavity has a typical effective optical path length of a few kilometres, the chiral optical rotation is dependent upon the direction of light propagation through the sample, and as such is suppressed when the linear polarized light passes back and forth through the cavity. Vaccaro and co-workers have circumvented this problem by inserting a pair of intra-cavity quarter-wave plates, allowing the chiral signal to be enhanced by a factor equal to the number of cavity round-trip passes, although, in addition, linear birefringence due to the intra-cavity optics is also increased^{17,18}.

More recently, bow-tie CRDP using pulsed lasers has been developed involving two counter-propagating linearly polarized beams, in which the effects of the intra-cavity birefringence are cancelled by means of a signal reversing technique and a reference Faraday rotation angle is induced by an intra-cavity magneto-optic crystal^{19–22}. In this case the optical rotation is then deduced from the two cavity ring-down signals without needing to remove the sample from the polarimeter. The pulsed-CRDPs utilize lasers that are typically expensive, relatively bulky and have large optical linewidths (\sim GHz or more). Multiple longitudinal and transverse mode excitation occurs when using

most pulsed lasers and can result in multi-exponential decays. Moreover, intensity fluctuations caused by interference can be superimposed upon the ring-down signal, potentially leading to a reduction in the sensitivity. Some of these problems can be mitigated by using narrow linewidth (MHz) single-longitudinal-mode continuous-wave (*cw*) lasers. Furthermore, the use of *cw* lasers offers the possibility of further enhancing the sensitivity of the CRDP methodology by effective mode-matching of light into a single cavity mode and increasing the intra-cavity power via locking the laser frequency to the cavity resonance²³. Finally, with the replacement of pulsed lasers with compact, relatively low cost, narrow linewidth, *cw* laser sources, *cw*-CRDP will become widely accessible for ultra-sensitive chirality measurements²³.

In this paper, we build upon the previous seminal studies on signal reversing CRDP with pulsed lasers¹⁹⁻²² and demonstrate CRDP in operation with a *cw* laser source. In particular, we show that electrical perturbation of the laser's injection current provides a robust and effective way of exciting cavity modes to optimise the polarization modulation depth and to improve sensitivity. In this paper we first present the principles of CRDP using a *cw*-laser and demonstrate the improvement in sensitivity via broadening of the laser linewidth caused by the application of a radio-frequency noise signal to the injection current. We then present the experimental arrangement of a new *cw*-CRDP apparatus operating at 730 nm to measure chiral optical rotation in different environments, including the pure vapour, open air, and the liquid phase. Both (+) and (−) enantiomers of α -pinene are used as test molecules to assess the performance of our polarimetry with detection limits in the range of 10^{-4} and 10^{-5} degrees per cavity pass depending upon the environment. The paper concludes with a summary of the device performance and some comments about future improvements and applications for the technology.

PRINCIPLES OF CW CAVITY RING-DOWN POLARIMETRY

The operational principles of *cw*-CRDP based on the signal-reversing technique are described here. Two counter-propagating linearly polarized laser beams, labelled as clockwise (CW) and counter-clockwise (CCW) beams are optically mode-matched with the TEM₀₀ mode of a bow-tie cavity that is constructed with four high reflectivity mirrors with an average reflectivity of R . Upon mode excitation and its subsequent cessation, caused by triggering the AOM to turn off, the time dependent intensity of the cavity output is an exponential function $I = I_0 e^{-t/\tau_0}$ with I_0 the incident light power and $\tau_0 \approx L/c (1 - R^4)$ the ring-down time with c the speed of light and L the cavity length. Figure 1(a) shows an example cavity ring-down signal with $\tau_0 = 4 \mu\text{s}$, generated by excitation of a single cavity (polarization) mode. A magneto-optic crystal (length l), typically Terbium Gallium Garnet (TGG), with a large Verdet constant V (ranging between a few tens to a few hundred $\mu\text{rad G}^{-1} \text{cm}^{-1}$ depending on the working wavelength) is introduced into one arm of the cavity. By applying a longitudinal magnetic field, B , to the crystal, the polarization axes of the counter propagating laser beams are rotated with the same Faraday rotation angle of $\phi_F = VBl$. The magnitude of ϕ_F is typically chosen to be a few degrees so as to dominate the linear birefringence induced by the cavity mirrors (typically less than 0.2°). Two polarizers are placed at the cavity

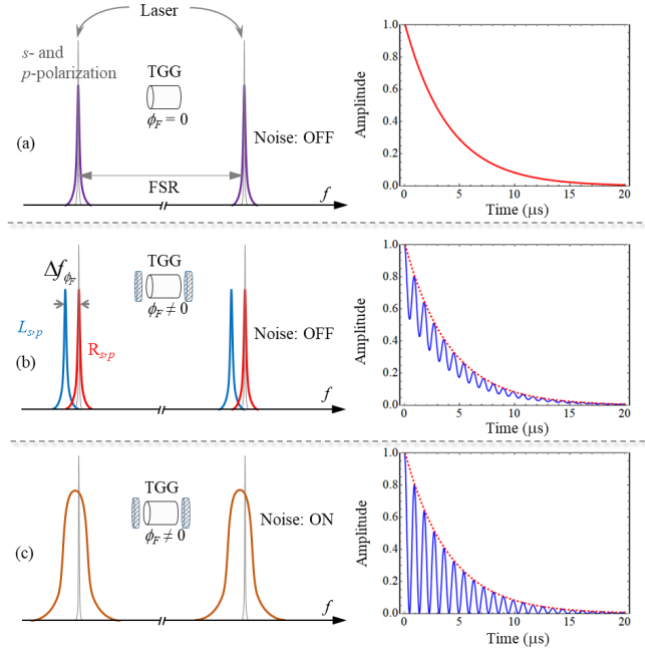


Figure 1. Principle of *cw*-CRDP based on a bow-tie cavity. Spectra of cavity resonances are shown on the left panels and cavity ring-down signals are shown on the right panels. (a) For the case of near-normal incidence of reflection on the cavity mirrors, the cavity resonances of the *p*- and *s*-polarization beams are near-degenerate. The red curve shows a simulated traditional ring-down trace with a ring-down time of $4 \mu\text{s}$. (b) In the presence of a longitudinal magnetic field, the TGG crystal displays circular birefringence. Due to the Faraday effect, each resonance is split into two orthogonal circularly polarized modes (*L*- and *R*-mode). A *cw* laser of linewidth narrower or comparable to the splitting can lead to both *L*- and *R*-modes contributing to the detected signal, but in an unpredictable way, causing the polarization-modulation depth to be reduced, as shown by the blue curve. (c) Once the laser linewidth is broadened and can cover the two non-degenerate modes, the modulation depth of the polarization beat frequency can approach unity, as illustrated by the blue curve. Simulation parameters: $\tau_0 = 4 \mu\text{s}$; $\omega = 2\pi f = 3.5 \times 10^6 \text{ rad/s}$; $C = 1.5$ for panel (b), and $C = 0$ for panel (c). The blue curves are calculated using Equation (1).

outputs to analyse the projection of the polarization states of the output beams and consequently a time-dependent signal is detected, that is an exponential ring-down signal superimposed with a periodic function,

$$I(t) = A e^{-\frac{t}{\tau_0}} [\cos^2(2\pi f t + \varphi) + C], \quad (1)$$

where A is the amplitude of the detected signal, $f = c\phi/2\pi L$ is the polarization beating frequency with ϕ the single-pass rotation angle, φ is the global phase offset (typically $\varphi = 0$), and C takes into account any reduction in the polarization-modulation depth (due to, for example, linear birefringence of mirrors, limited bandwidth detection, and imperfections of the polarization alignment).

Once a chiral sample is introduced into the cavity, a chiral optical rotation, ϕ_C , occurs with an opposite sign for each beam as it is determined by the propagation direction of the light. By contrast, the sign of the offset rotation ϕ_F is the same for both beams and depends on the direction of the magnetic field. After each cavity

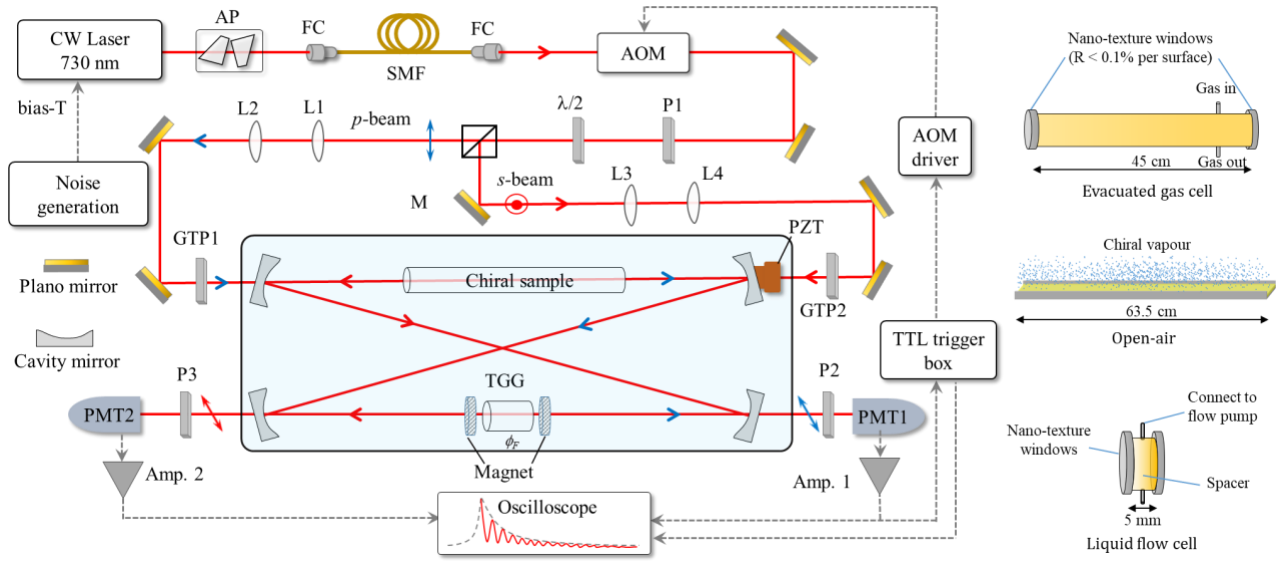


Figure 2. Experimental arrangement for cavity ring-down polarimetry at 730 nm. Two counter-propagating linearly polarized beams labelled as the p - and s -polarized beam are mode-matched with the TEM_{00} mode of a bow-tie cavity that is constructed by four highly plano-concave reflective mirrors ($R \sim 99.985\%$). A Terbium Gallium Garnet crystal (TGG) with anti-reflection coating on both sides ($R < 0.1\%$) is placed in one arm of the cavity while the chiral sample is placed in the other arm. Optical rotation measurements can be performed in the gas-phase, in the open air, and in the liquid phase. The transmitted beams are detected by two photo-multiplier tubes (PMT) and their polarization states are analysed by two Glan-Taylor polarizers. Experimental data is acquired by a high-speed oscilloscope (2 GS/s). AP: anamorphic prism pair; FC: fibre coupler; SM: single-mode fibre; AOM: acousto-optic modulator; P: plate polarizer; M: mirror; L: lens; PMTs: photomultiplier tube; Amp.: Amplifier.

round-trip, the polarization direction of the laser beams is thus rotated by an amount given as the sum $\phi_{CW} = \phi_F + \phi_C$ (for the CW beam) and the difference $\phi_{CCW} = \phi_F - \phi_C$ (for the CCW beam) of ϕ_F and ϕ_C . By fitting Equation (1) to the detected ring-down signals, the polarization beating frequencies are consequently determined using the following formulae,

$$f_{CW}(\pm B) = \pm f_{\phi_F} + f_{\phi_C} = \frac{c}{2\pi L} (\pm \phi_{\phi_F} + \phi_{\phi_C}) \quad (2)$$

and

$$f_{CCW}(\pm B) = \pm f_{\phi_F} - f_{\phi_C} = \frac{c}{2\pi L} (\pm \phi_{\phi_F} - \phi_{\phi_C}). \quad (3)$$

The frequency difference between the two beating frequencies $\Delta f(\pm B) = |f_{CW}(\pm B) - f_{CCW}(\pm B)|$ therefore yields the optical rotation of the chiral sample. If the CW beam has the same propagation direction as the magnetic field, the chiral optical rotation is given by

$$\phi_C = \frac{\pi L}{c} (f_{CW} - f_{CCW}). \quad (4)$$

One potentially confounding factor arises from the circular birefringence displayed by the magneto-optic crystal in the presence of a longitudinal magnetic field (the Faraday effect²⁴). Each cavity resonance is separated into two circularly polarized resonances, one for the left circularly polarized mode (L -mode) and other one for the right circularly polarized mode (R -mode) with a frequency splitting given by $\Delta f_{\phi_F} = c\phi_F/\pi L$ (see Figure 1(b)). Most previous cavity-based polarimetry has been demonstrated with pulsed laser sources whose linewidths can cover several cavity free spectral ranges¹⁹⁻²². Therefore, these non-degenerate circularly polarized modes can be simultaneously excited in the cavity and good contrast in the modulation-polarization signal observed, *i.e.* the modulation depth approaches unity ($C \sim 0$). This is not the case when using a *cw* laser and where the frequency splitting is larger than both

the laser and cavity linewidths. Typically, in such a case, with a linearly polarized source, it is problematic to simultaneously excite these modes so as to result in no net preference for one sense of circular polarization. Thus, the ring-down signal can be dominated by one of the two circularly polarized modes, resulting in a reduction in the modulation-polarization depth ($C > 0$) and limiting the detection sensitivity. A similar effect for the two-mirror configuration has been recently demonstrated by Bougas and co-workers²³. As an example of this effect, we plot in Figure 1(b) a calculated cavity ring-down signal (solid blue curve) with a polarization beating angular frequency of $\omega = 2\pi f = 3.5 \times 10^6$ rad/s, and $C = 1.5$. This reduced polarization modulation can be mitigated by reducing the frequency splitting Δf_{ϕ_F} between the two circularly polarized modes; however, the Faraday offset angle is typically required to be at least ten times larger than the intra-cavity linear birefringence (typically $0 - 0.2^\circ$) to prevent the depolarization effect of the birefringence on the measurement of the two oscillating frequencies^{19,25}.

Another possible solution to increasing the polarization modulation (and hence sensitivity) is to use a *cw* laser exhibiting a relatively large linewidth (few tens of MHz) that is a few times larger than the frequency splitting. In this case, an injection of a radio-frequency white noise signal to the laser via the laser current leads to the perturbation of the laser frequency (see next section for more details) in a controllable and tuneable manner²⁶⁻²⁸. As shown in Figure 1(c), the laser linewidth has been broadened by an additional noise signal and thus both circularly polarized modes are equally excited in the cavity (corresponding to a mode of the linear polarization), making the amplitude modulation approach unity.

EXPERIMENTAL SETUP

Figure 2 shows a schematic of the experimental setup of our polarimeter, which allows optical rotation measurement of chiral samples to be conducted in both gas and liquid phases. A bow-tie cavity is formed by four high-reflectivity concave mirrors (Layertec, diameter of 25.4 mm, and radius of curvature of 1 m). Each mirror has a reflectivity of *ca.* 99.985% over the wavelength range 730 to 790 nm. One of the mirrors is mounted on a piezo-electric transducer (PZT), used for scanning the cavity length. The bow-tie cavity has a total length of 3046 ± 4 mm (width and length separations of ~ 760 and ~ 68 mm, respectively), corresponding to a free spectral range of ~ 98 MHz. The light source is a *cw* external-cavity diode laser (Sacher Lasertechnik, linewidth < 1 MHz) emitting in the range of 720–740 nm with a maximum power of 50 mW. Its absolute frequency is monitored by an optical wavemeter (Burleigh, WA-1000). The laser beam is first directed through a pair of anamorphic prisms (Thorlabs, PS871-B) to circularise the elliptical beam before coupling into a single-mode optical fibre (Thorlabs, P3-630A-FC5) that provides a Gaussian-shaped beam, mimicking the TEM₀₀ mode of the cavity. After coupling to free-space, the light beam is directed through an acousto-optic modulator (AOM, MT80-A1-IR, AA Opto-Electronic), used to switch off the laser beam with a fall time of ~ 80 ns. The resulting first order diffraction from the AOM, with a power of ~ 3 mW, is directed to the spectroscopic setup. The AOM driver (MODA80-1W/2W, AA Opto-Electronic) is controlled by a home-made TTL trigger box which acts as the master trigger to generate cavity ring-down signals following intracavity power build-up. A half-wave plate ($\lambda/2$, B-Halle) and a polarizing beam-splitting cube (Thorlabs, PBS252) are used in tandem to separate the light beam into two linearly polarized beams (*p*- and *s*-polarized beams or CW and CCW beams). A set of lenses is used for matching the spatial profile of the two counter-propagating beams to the TEM₀₀ cavity mode. The polarization states of the light beams are filtered and fixed by two Glan-Taylor polarizers (GT10-B, Thorlabs) with an extinction ratio of $\sim 10^5$.

A 3 mm-thick TGG crystal (MolTech GmbH) with anti-reflection (AR) coated faces is placed in one arm of the cavity to induce a large offset rotation angle, ϕ_r . The TGG crystal has a Verdet constant of $V \simeq 100 \mu\text{rad G}^{-1}\text{cm}^{-1}$ at 730 nm and a reflectivity of $R \sim 0.07\%$ for each surface. The ring-down time is measured to be $\sim 5 \mu\text{s}$. Typically, a large Faraday rotation, $\phi_r \sim 1.7 - 3.4^\circ$ is generated by applying a magnetic field 0.1 – 0.2 T to the crystal, using two permanent (ring) neodymium magnets. The chiral sample is introduced to the other arm of the cavity. Two plate polarizers P2 and P3 (Thorlabs, LPNIR100-MP2) were placed at the cavity outputs to analyse the polarization states of the two counter-propagating beams. The cavity ring-down traces are detected by two photomultiplier tubes (Hamamatsu H10721-20, rise time of ~ 0.6 ns). The detected signals are amplified (FEMTO DHPA-100, bandwidth of 200 MHz) and acquired by a high-speed oscilloscope (MSO Infiniium Oscilloscope Agilent, bandwidth of 1 GHz, 2 GS/s sampling) that allowed the detected traces to be averaged. As described in the previous section, each cavity resonance is split into two circular polarisation states by the Faraday effect with a frequency splitting of ~ 2.5 MHz, causing the amplitude modulation depth to be reduced. During acquisition, a broadband radio-frequency noise signal, generated by a noise generator (Noise Brick, 50 kHz–500 MHz) and amplified up to +25 dB by a home-made voltage amplifier, is mixed with the drive current of the laser via a bias-T. The noise-

induced broadened linewidth of the laser is estimated to be ~ 10 MHz, determined using an optical spectrum analyser (Thorlabs, SA30-73). The optimum rf modulation produces a broadened linewidth that allows both circularly polarized states (*L*- and *R*-mode) to be efficiently and reproducibly excited in the cavity. To determine the optimum rf modulation, we varied the amplitude of the white-noise signal, broadening the laser linewidth to optimise the apparent modulation depth and then fine-tuned this by determining the corresponding value of *C* by fitting the model (given by equation (1)) to the acquired trace. The optimized noise amplitude is found to be ~ 200 mV (peak-to-peak).

Cavity ring-down traces are measured at regular intervals, induced by applying a triangular-wave signal with a frequency of 30 Hz to the PZT and scanning the cavity length. The cavity length dither amplitude is large enough to ensure that several cavity resonances cross the laser frequency in each cycle. As illustrated in Figure 2, the detected signal from PMT1 is sent to a home-made trigger box to rapidly switch off the laser beam and allow measurement of ring-down events. Cavity ring-down signals are typically recorded and averaged over 2000 events in a total time of 60 seconds.

RESULTS AND DISCUSSIONS

We have used *cw*-CRD polarimetry to carry out optical rotation measurements on samples of (+)- and (–)- α -pinene (Sigma Aldrich), of optical purity *ee* $\geq 97\%$, in different environments: controlled-pressures of the pure vapour using an evacuated intra-cavity sample cell, vapour/air mixtures, and mixtures of the liquid sample and solvent using an intra-cavity liquid flow cell.

Gas phase optical rotation measurements of pure vapour

A 45 cm long gas cell was inserted in one arm of the cavity. It is enclosed by AR nanotextured fused silica windows (Newport, 10Q20RAR.L) with a reflectivity lower than 0.1% per surface. The cell was evacuated below 10^{-5} mbar by a turbo pump (Leybold, TurboVac 360) and the working gas pressure measured by a capacitance manometer (CERAVAC, CTR100, pressure range of 100 Torr). The chiral samples were contained in a glass reservoir (MDC Vacuum, KSEG-075) and vapour injected into the chamber using a dosing valve (Swagelok, SS-4BMRG) to produce a static sample. A magnetic field of ~ 0.16 T was applied to the TGG crystal, corresponding a Faraday rotation angle per cavity round-trip of $\sim 2.6^\circ$. The pressure-controlled vapour measurements were carried out with only one magnetic field direction (+B). A typical averaged polarization modulated cavity ring-down signal for the CW and CCW beams propagating in an empty cavity is shown in Figure 3(a). The relative intensity of light transmitted is plotted as a function of time, where $t = 0$ corresponds to the triggering point. The ring-down time for both channels is found to be $\sim 2.2 \mu\text{s}$, at least twice as large as in previous studies^{19,20,22}, corresponding to ~ 220 round-trips inside the cavity and an effective path length of ~ 99 m.

In the analysis, all data points within an averaged ring-down signal are assigned the same error bar which is the standard deviation of the residuals obtained after fitting a second-order polynomial function to a small portion of the baseline signal. The experimental error is typically *ca.* 0.1% of the ring-down amplitude. For this apparatus we find that without added noise, a fit to the cavity signal yields $C \sim 7$, which qualitatively manifests as a modulation about half as large as that presented in figure 1b.

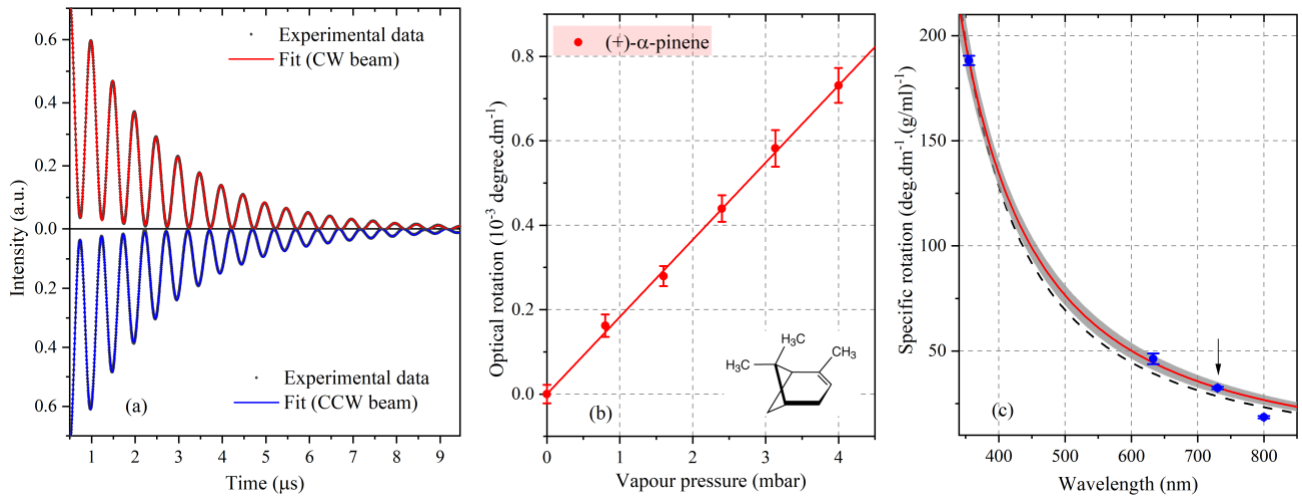


Figure 3. Gas-phase optical rotation measurements of (+)- α -pinene vapour at different pressures. (a) Typical cavity ring-down signal for the CW and CCW beams at zero pressure (black points). The red and blue solid curves are the fit of the amplitude modulation model to the data. The modulation depth of the polarization beat frequency approaches unity and the ring-down time is found to be ~ 2.2 μ s for these beams. (b) Variation of optical rotation of (+)- α -pinene vapour as a function of pressure. Each data point and its error bar are given by the mean and the standard error of the 20 measurements at a given pressure, respectively. The red line is a weighted linear fit to the data. Experimental parameters: magnetic field: ~ 0.16 T giving $\phi_F \sim 2.6^\circ$, 2000 events averaged over 60 s. (c) Variation of the specific rotation of (+)- α -pinene as a function of wavelength (blue points). The black arrow indicates the optical rotation of (+)- α -pinene at 730 nm measured by our *cw*-CRDP. The red solid and black dashed curves are the fit of the wavelength dependence of the optical rotation to the data (see text for details) and the grey area is the mean prediction band resulting from the fit (red curve) with a confidence level of 0.9.

As shown in Figure 3(a), with the application of optimised rf modulation, the polarization-modulation depth approaches unity ($C < 0.03$). The red and blue solid curves in Figure 3 are the fits of the amplitude-modulated model given by Equation (1) to the CW and CCW ring-down data, resulting the reduced chi-square values of ~ 1 .

For a given pressure, we carried out 20 measurements (over a period of 20 minutes) and determined the optical rotation using Equation (5). The uncertainty on the chiral rotation angle ϕ_c for each measurement can be calculated from the fitting error bars of f_{CW} and f_{CCW} (typically ~ 75 μ deg per round trip pass, error bar of f_{CW} and $f_{CCW} \sim 30$ Hz). We therefore estimate the chiral rotation and the associated uncertainty for a given pressure by calculating the weighted mean of the 20 measurements and the corresponding standard error (uncertainties calculated from the fit error bars of f_{CW} and f_{CCW} are used to calculate the weights). Moreover, in our current setup the magnetic field is not perfectly uniform (dropping by 5-10% at a distance of 1 cm away from the centre point between the two magnets). If the two counter-propagating beams are not perfectly overlapped with respect to the TGG crystal, and the optical rotation ϕ_F is expected to be slightly different for each propagation direction, resulting in an offset frequency δ between f_{CW} and f_{CCW} . This effect is observable in Figure 3(a) where the maxima and minima for the CW and CCW beams occur at different time points. The offset frequency, δ , is measured to be 7.34 ± 0.05 kHz. Typically, the offset frequency does not change even when the magnitude of the field has a small variation caused by any temperature drift or mechanical vibration. In the case of a positive B-field (defined as when the CW beam propagates with the same direction of the magnetic field), the chiral optical rotation is therefore determined by the following expression,

$$\phi_c = \frac{\pi L}{c} (f_{CW} - f_{CCW} - \delta). \quad (5)$$

Figure 3(b) shows the optical rotation per unit length of (+)- α -pinene as a function of pressure (the length of the gas cell is 44.4 ± 0.1 cm). During the acquisition, the pressure variation is less than 2%. The optical rotation precision is ~ 100 μ deg/pass, determined from the mean of error bars of ϕ_c at pressures below 1.0 mbar and is similar to that reported in recent studies with a pulsed laser²².

The red solid line in Figure 3(b) is the weighted fit to the data, confirming the linear dependence between the chiral rotation angle and pressure and yielding a slope of 0.1804 ± 0.0034 mdeg dm⁻¹ mbar⁻¹ for (+)- α -pinene. The gas-phase specific rotation of (+)- α -pinene is determined to be $+32.4 \pm 0.6$ deg dm⁻¹ (g/ml)⁻¹ at a wavelength of 730 nm and a temperature of 22°C. To our knowledge, these are the first measurements for the specific rotations of (+)- α -pinene in the gas-phase at 730 nm. Previously, the specific rotation of (+)- α -pinene has been reported to be $+188.2 \pm 2.2$ deg dm⁻¹ (g/ml)⁻¹ at 355 nm and $+46.3 \pm 2.5$ deg dm⁻¹ (g/ml)⁻¹ at 633 nm by Vaccaro *et al.*^{17,18} at 25°C; $+18.57 \pm 0.57$ deg dm⁻¹ (g/ml)⁻¹ at 800 nm by Sofikitis *et al.*¹⁹ at 19°C. In Figure 3(c), we plot the wavelength dependence of the optical rotation of (+)- α -pinene (blue circles). Where, for completeness, we have adjusted the optical rotation values for temperature using the temperature dependent (and solvent independent) optical rotation measured by Vaccaro and co-workers²⁹ for α -pinene ($< \sim 0.005$ deg dm⁻¹ (g/ml)⁻¹ (°C)⁻¹, extrapolated by us to 730 nm), although we note that these corrections lie well within the reported precision of the measurements. Noting that there are also weak electronic transitions at ~ 220 nm and 184 nm in α -pinene, if we assume that the optical rotation is dominated by the

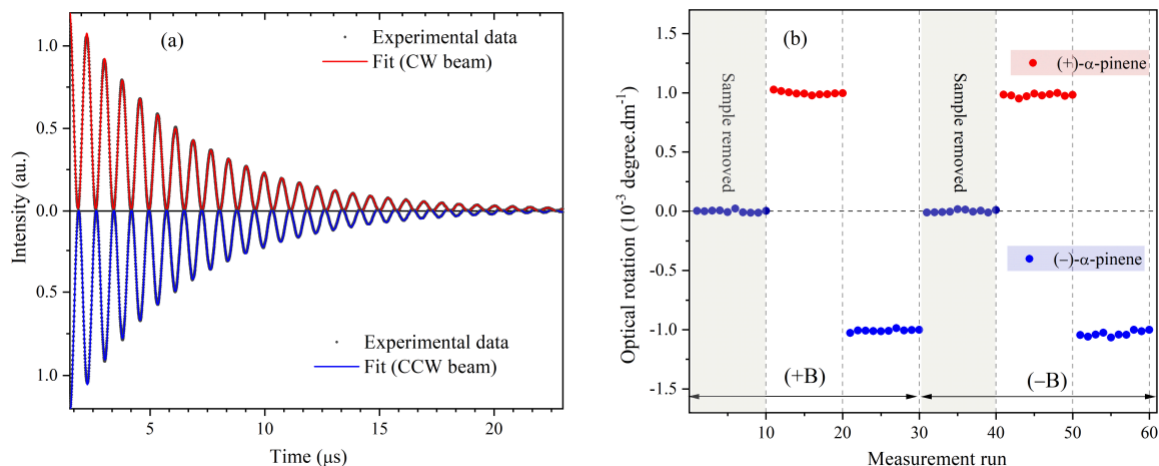


Figure 4. Optical rotation measurement of open-air vapour mixtures of (+)- and (-)- α -pinene. (a) Typical cavity ring-down signal for the CW and CCW beams for the open-air measurement. The modulation depth of the polarization beat frequency approaches unity and the ring-down time is found to be $\sim 5 \mu\text{s}$ for these beams. (b) Open-air optical rotations of (+)- and (-)- α -pinene for both directions of magnetic field +B and -B. Experimental parameters: magnetic field: $\sim 0.13 \text{ T}$ giving $\phi_F \sim 2.2^\circ$, 2000 events averaged over 60 s.

influence of the intense $\pi \rightarrow \pi^*$ electronic transition around 200 nm, then the optical rotation dispersion (ORD) can be modelled according to $[\alpha]_\lambda^T = A_T / (\lambda^2 - \lambda_0^2)$, where λ_0 is the wavelength associated with the intense UV transition responsible for the measured rotation and A_T is the temperature dependent amplitude³⁰. The black dashed curve in Figure 3(c) is a weighted fit of this simpler ORD model to all data points. Perhaps surprisingly (but bearing in mind that this is a simple model), we find that the difference between the reported optical rotations at 633, 730, and 800 nm, and those calculated from the best fit curve are a few times larger than the reported error bars. We note however that after removing the data point at 800 nm from the fit, a best match between the model and the data is obtained and is shown by the red solid line in Figure 3(c). The resulting closest UV transition wavelength and the optical rotation amplitude are found to be $\lambda_0 = 202 \pm 4 \text{ nm}$ and $A_T = (1.60 \pm 0.03) \times 10^7 \text{ deg dm}^{-1} (\text{g/ml})^{-1} \text{ nm}^2$, respectively. The former is consistent with the centre wavelength of 201.2 nm of the intense $\pi \rightarrow \pi^*$ electronic transition in α -pinene^{31,32}. The grey area encompassing the red line (in figure 3(c)) represents a 90% confidence level.

Open-air measurement

Cavity ring-down polarimetry has also been used to measure optical rotation by open-air vapours of (+)- and (-)- α -pinene. In this case, a 63.5cm-length cylindrical glass tube (internal diameter of 1 cm) with two open ends was introduced into one arm of the cavity. A small amount of liquid sample was introduced along the entire length of the bottom inner surface of the glass tube, directly below one of the optical arms of the cavity. Six replicate sets of ten experiments were undertaken with both directions of the magnetic field. For each field direction, we first carry out a set of ten experiments without the chiral sample (glass tube removed) to determine the offset frequency, δ . After inserting the cell filled with chiral sample into the cavity, the second and third set of ten experiments on (+)- and (-)- α -pinene are performed, respectively. Figure 4(a) shows typical ring-down signal from the CW and CCW beams for the open-air measurement (black points) with no sample present. The ring-

down time is found to be $\sim 5 \mu\text{s}$ for both channels, corresponding to ~ 500 round-trips inside the cavity and an effective path length of $\sim 317 \text{ m}$. The increased pathlength reflects the reduced optical losses in comparison to the case where the sealed gas cell was in the cavity.

We determine the four oscillating frequencies $f_{CW(+B)}$, $f_{CW(-B)}$, $f_{CCW(+B)}$, and $f_{CCW(-B)}$ by fitting the modulated-amplitude model to the data (Equation (1) and red and blue curves in figure 4(a)). Figure 4(b) shows the optical rotation per unit length of vapour of (+)- and (-)- α -pinene, measured at a temperature of 23°C . As expected, the optical rotations resulting from each direction of the magnetic field are coincident for a given enantiomer. By taking into account all measurements for both positive and negative B-field configurations, the open air optical rotation at 730 nm and at $\sim 23^\circ\text{C}$ is found to be $+0.989 \pm 0.004 \text{ mdeg dm}^{-1}$ for (+)- α -pinene and $-1.021 \pm 0.005 \text{ mdeg dm}^{-1}$ for (-)- α -pinene. These values are consistent with both samples having *ee* values of at least 97%. The optical rotation precision is around $30 \mu\text{deg/pass}$. The vapour pressure of both enantiomers at 23°C is *ca.* 5.2 mbar³³. The specific rotation of (+)- and (-)- α -pinene can therefore be estimated to be *ca.* $+34$ and $-35 \text{ deg dm}^{-1} (\text{g/ml})^{-1}$, respectively, and are slightly higher than the results obtained from the controlled-pressure measurement on the pure vapours. We note however that this is a crude estimate, because the interaction region between the vapour and the optical path is poorly defined, as both ends of the tube are open and we expect the vapour to diffuse (albeit slowly) out of the ends. Despite our best efforts to hastily conclude the experiments we estimate that this could contribute a 10% uncertainty in the effective interaction length. A further minor consideration is that the partial pressure of the vapours may be subtly shifted from that of the pure enantiomer due to non-ideality arising from molecular interactions.

Liquid phase optical rotation measurement

To facilitate optical rotation measurements of liquid phase pinene, a 5 mm thick flow cell was introduced into one arm of

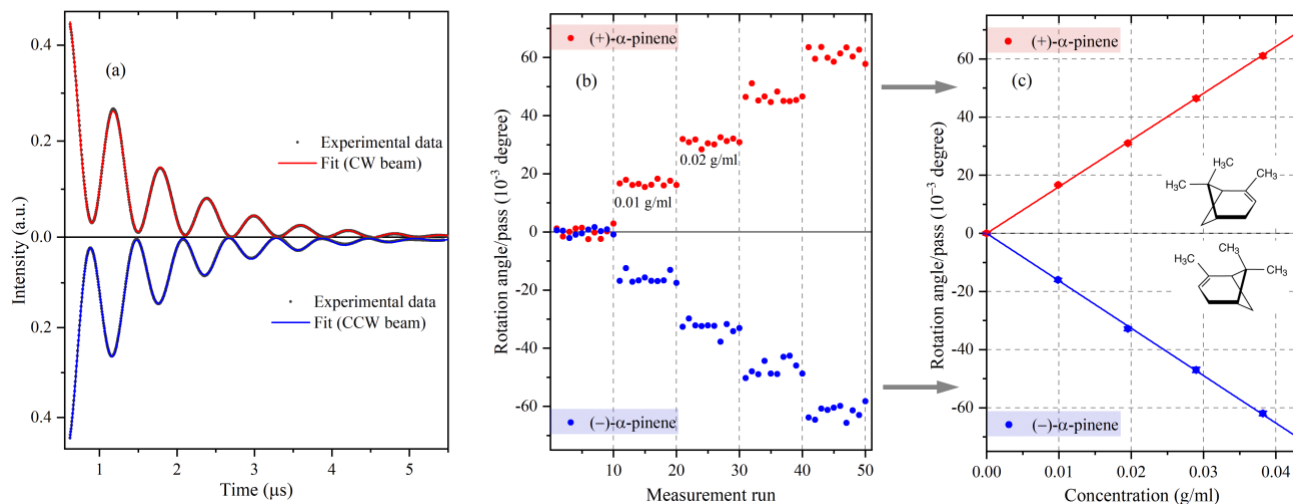


Figure 5. Liquid-phase optical rotation measurement of (+)- and (-)- α -pinene in methanol at different concentrations. (a) Typical experimental cavity ring-down signals (black points) for the CW and the CCW beams at zero concentration. The red and blue curve are the fit of the model given by Equation (6) to the data. The ring-down time is found to be $\sim 1.2 \mu\text{s}$ for both signals. (b) Optical rotation of (+)- and (-)- α -pinene at concentrations ranging between 0 and 0.04 g/ml are injected into the cell using a flow pump. (c) Variations of rotation angle per round-trip pass in the cavity as a function of concentration (red points for (+)- α -pinene and blue points for (-)- α -pinene). Each data point and its error are the average and the standard error of ten data sets at a given concentration, respectively. The red and blue lines are weighted linear fits to the data. Experimental parameters: magnetic field: $\sim 0.13 \text{ T}$ giving $\phi_F \sim 2.2^\circ$, non-chiral sample, 2000 events averaged over 60 s.

the cavity. It consists of two AR nanotextured fused-silica windows (Newport, 10Q20RAR.L) mounted on two kinematic cage-compatible mounts (Thorlabs, KC1/M) and separated by a spacer. Chiral solutions with different concentrations of pinene dissolved in methanol were injected into the cell using a flow pump (Masterflex, 7518-10) with a flow rate of 0.07 ml/s. Again, a magnetic field of $\sim 0.13 \text{ T}$ was applied to the TGG crystal, corresponding to a Faraday rotation of $\sim 2.2^\circ$ with the same sense as for the CW laser beam. As for the pressure-controlled vapour measurements, we performed the liquid phase measurements with only one direction of magnetic field (+B). In Figure 5(a), we plot a typical cavity ring-down signal (black points) obtained when the cell is filled with pure methanol. Each spectrum is an average of 2000 events recorded in 60 seconds. The optical loss on the nanotextured fused-silica/methanol interface is found to be less than 0.2%. The ring-down time of $\sim 1.2 \mu\text{s}$ corresponds to ~ 120 round-trips inside the cavity and an effective path length through the liquid sample of $\sim 60 \text{ cm}$, a few times larger than previously reported^{20,21}. In this case a best-matching model to the detected signal is given by the following expression, which is a variant of equation (1):

$$I(t) = Ae^{-t/\tau_0}[\cos^2(2\pi f t + \varphi) + D(t)], \quad (6)$$

but includes a term $D(t)$, which is a second-order polynomial modelling a non-linear baseline specific to the liquid phase measurements. We find that for all our CRDP measurements there is an initial period in the signal ($\sim 300 \text{ ns}$) that is influenced by the finite time required to trigger and switch off the AOM. To make sure that our analysis is not influenced by this, we cut off the first 0.6 μs of data. For the liquid phase measurements this is exacerbated by the use of two 1.9 MHz low pass filters (Minicircuits, one for each channel) that we have utilised because of the lower signal-to-noise ratio in these data. Beyond the 0.6 μs cut-off, the filters have introduced a small residual non-linear

baseline which we have modelled with the second order polynomial $D(t)$. The red and blue solid curves are the fit of the model given by Equation (6) to the data for the CW and CCW beams, respectively.

We follow the same procedure as in the gas-phase measurement to determine the optical rotations and their corresponding uncertainties for each enantiomer in the solution. Figure 5(b) shows the variation of rotation angle per cavity pass of (+)- and (-)- α -pinene as a function of concentration between 0 and 0.04 g ml⁻¹. For each given concentration, we carry out 10 measurements and determine the rotation angle per pass using Equation (5). Each data point and its error bar in Figure 5(c) are given by the weighted mean and the standard error of the ten measured chiral rotation angles. The optical rotation precision is calculated as the average of the error bars shown in Figure 5(c) and varies as a function of concentration; at the lowest concentrations the limit is $\sim 180 \mu\text{deg/pass}$, increasing up to as much as $700 \mu\text{deg/pass}$. This variation reflects the reduction of ring-down time in the cavity due to increased absorption and/or refractive index mismatch by each enantiomer as its concentration increases. In Figure 5(c), the red and blue solid lines are the fit to the data, and again confirm the linear dependence between the rotation angle per pass and concentration. The resulting slopes are found to be $1.614 \pm 0.018 \text{ deg (g/ml)}^{-1}$ for (+)- α -pinene and $-1.631 \pm 0.013 \text{ deg (g/ml)}^{-1}$ for (-)- α -pinene. The specific rotations of (+)- and (-)- α -pinene are found to be $32.3 \pm 0.3 \text{ deg dm}^{-1} (\text{g/ml})^{-1}$ and $-32.6 \pm 0.3 \text{ deg dm}^{-1} (\text{g/ml})^{-1}$ at a wavelength of 730 nm and a temperature of 22°C , respectively. We therefore find that the optical rotation values of the solution measurement are the same (within error) as those determined from the gas-phase measurement. Although solvents which can exhibit hydrogen bonding and have a high dielectric constant may modify the optical rotation dispersion

curve of chiral molecules, here we observe no such net effects. This is not unprecedented, there exist other cases for which the chiral rotations resulting from gas and solution measurements are identical¹⁷. To our knowledge, there are only two studies that use the pulsed source-based CRDPs with intra-cavity flow cells for detecting chiral optical activity in solution phase with reported ring-down decay times of a few hundreds of ns. We note that we report similar sensitivities for optical rotation in solution compared to previous studies²¹, but that perhaps as a consequence of better apparatus stability and reproducibility, possibly combined with lower optical losses (ringdown times > 1 μ s) which results in a larger dynamic range over which measurements can be made, we are able to report a precision in the measurement of the specific rotation of 0.3 deg dm⁻¹(g/ml)⁻¹, nearly one order magnitude better than recently reported work^{20,21}.

CONCLUSION

We have presented the development of a new sensitive cw-CRD polarimeter for measuring optical activity of chiral molecules. The methodology relies upon broadening of the laser linewidth to non-selectively, regularly and simultaneously excite both non-degenerate L- and R-polarization modes, intrinsic to this modality, while retaining the sensitivity inherent to cavity enhanced techniques. We have demonstrated that the use of novel optical components such as nano-textured low-loss windows are suitable for intracavity operation enabling liquid phase measurements without the necessity for index matching. The apparatus/methodology is robust: the laser and cavity require no active stabilization; the method is easily implemented and can be used to develop polarimetry at any available wavelength in the near UV, visible and near-infrared spectral windows, all attractive features for potential field deployment. The cw-CRD technique has been demonstrated here at 730 nm and the optical rotation measured of enantiomers of α -pinene in both the gas and liquid phases.

The limits of detection reported here are ~30 μ deg/pass and ~180 μ deg/pass for the gas and liquid phase measurements, respectively, over a one minute acquisition time. This compares favourably with previous measurements although we note that with active laser – cavity locking better sensitivities are achievable: Visschers *et al.*²³ have recently reported very high sensitivity to Faraday optical rotation with such a linear CRDP device but on a solid-phase sample of SiO₂ (488 nrad/Hz^{1/2}/roundtrip). However, this requires a highly stabilised system and cavity resonance to be excited and it is not trivial to implement an equivalent modification to our scheme, or indeed whether the extra sensitivity imbued by the complexity would transfer (quantitatively) to, for example, a device for measuring liquid phase optical rotation. Nevertheless, we may gain extra sensitivity here with the provision for fast modulation of the magnetic field, to help cancel out background effects, and certainly, the precision of the gas phase measurements can be improved with better temperature stabilisation which minimizes the variation of the Faraday offset. The uncertainties in our measurements of specific rotation are better than 0.6 deg dm⁻¹(g/ml)⁻¹ for the gas phase and 0.3 deg dm⁻¹(g/ml)⁻¹ for the liquid phase. Chiral optical activity measurements with CRDPs at this level of accuracy are scarce, especially for the solution phase, and to our knowledge, there have been only two approaches to optical rotation measurement in solution reported¹⁹⁻²¹ (by the same

group), one of which uses an evanescent wave scheme. Of the other, which is a direct flow-cell measurement (comparable to our measurement), the reported uncertainty of 2.3 deg dm⁻¹(g/ml)⁻¹. This work is a part of our on-going development of highly sensitive polarimetry for detection of enantiomeric excesses of an amino acid solution flowed through mineral clay that can amplify chiral asymmetry³⁴ and promote peptide bond formation³⁵.

AUTHOR INFORMATION

Corresponding Authors

Dang-Bao-An Tran – Department of Chemistry, Physical and Theoretical Chemistry Laboratory, University of Oxford, South Parks Road, Oxford, OX1 3QZ, United Kingdom; Permanent address: Department of Physics, Ho Chi Minh City University of Education, Ho Chi Minh City, Vietnam
E-mail: an.tran@chem.ox.ac.uk

Grant A. D. Ritchie – Department of Chemistry, Physical and Theoretical Chemistry Laboratory, University of Oxford, South Parks Road, Oxford, OX1 3QZ, United Kingdom
E-mail: grant.ritchie@chem.ox.ac.uk. Phone: +44 (0)1865 285723. Fax: +44 (0)1865 275410

Authors

Katherine M. Manfred – Department of Chemistry, Physical and Theoretical Chemistry Laboratory, University of Oxford, South Parks Road, Oxford, OX1 3QZ, United Kingdom; Present address: Wolfson Atmospheric Chemistry Laboratories, Department of Chemistry, University of York, YO10 5DD, UK

Robert Peverall – Department of Chemistry, Physical and Theoretical Chemistry Laboratory, University of Oxford, South Parks Road, Oxford, OX1 3QZ, United Kingdom

Author Contributions

The manuscript was written through contributions of all authors. All authors have given approval to the final version of the manuscript.

Notes

The authors declare no competing financial interest.

ACKNOWLEDGMENT

The work was funded by the European Commission Horizon 2020, ULTRACHIRAL Project (Grant No. FETOPEN, ID number: 737071). The authors would like to thank Prof. Gus Hancock for valuable comments. DBA Tran would like to thank Dr. Benoit Darquié for his discussion of the experimental setup.

REFERENCES

- (1) Viedma, C.; Cintas, P. *Israel Journal of Chemistry* **2011**, *51*, 997-1006.
- (2) Corradini, R.; Sforza, S.; Tedeschi, T.; Marchelli, R. *Chirality* **2007**, *19*, 269-294.
- (3) Bouchiat, M. A.; Bouchiat, C. *J. Phys. France* **1974**, *35*, 899-927.
- (4) Bouchiat, M.-A.; Bouchiat, C. *Rep. Prog. Phys.* **1997**, *60*, 1351-1396.
- (5) Darquié, B.; Stoeffler, C.; Shelkovnikov, A.; Daussey, C.; Amy-Klein, A.; Chardonnet, C.; Zrig, S.; Guy, L.; Crassous, J.; Soulard, P.; others. *Chirality* **2010**, *22*, 870-884.

- (6) Cournol, A.; Manceau, M.; Pierens, M.; Lecordier, L.; Tran, D. B. A.; Santagata, R.; Argence, B.; Goncharov, A.; Lopez, O.; Abgrall, M.; others. *Quantum Electronics* **2019**, *49*, 288.
- (7) Patterson, D.; Schnell, M.; Doyle, J. M. *Nature* **2013**, *497*, 475-477.
- (8) Shubert, V. A.; Schmitz, D.; Patterson, D.; Doyle, J. M.; Schnell, M. *Angewandte Chemie International Edition* **2014**, *53*, 1152-1155.
- (9) Rhee, H.; June, Y.-G.; Lee, J.-S.; Lee, K.-K.; Ha, J.-H.; Kim, Z. H.; Jeon, S.-J.; Cho, M. *Nature* **2009**, *458*, 310-313.
- (10) Tang, Y.; Cohen, A. E. *Science* **2011**, *332*, 333-336.
- (11) Riehl, J. P.; Muller, G. *Comprehensive chiroptical spectroscopy* **2012**, *1*, 65-90.
- (12) Janssen, M. H. M.; Powis, I. *Phys. Chem. Chem. Phys.* **2013**, *16*, 856-871.
- (13) Polavarapu, P. L. *Chirality* **2002**, *14*, 768-781.
- (14) Stephens, P. J.; Devlin, F. J.; Cheeseman, J. R.; Frisch, M. J.; Bortolini, O.; Besse, P. *Chirality* **2003**, *15*, S57-S64.
- (15) Stephens, P. J.; McCann, D. M.; Cheeseman, J. R.; Frisch, M. J. *Chirality* **2005**, *17*, S52-S64.
- (16) Polavarapu, P. L. In *Chiral Analysis*; Elsevier, 2006, pp 461-504.
- (17) Müller, T.; Wiberg, K. B.; Vaccaro, P. H. *J. Phys. Chem. A* **2000**, *104*, 5959-5968.
- (18) Wilson, S. M.; Wiberg, K. B.; Cheeseman, J. R.; Frisch, M. J.; Vaccaro, P. H. *J. Phys. Chem. A* **2005**, *109*, 11752-11764.
- (19) Sofikitis, D.; Bougas, L.; Katsoprinakis, G. E.; Spiliotis, A. K.; Loppinet, B.; Rakitzis, T. P. *Nature* **2014**, *514*, 76-79.
- (20) Bougas, L.; Sofikitis, D.; Katsoprinakis, G. E.; Spiliotis, A. K.; Tzallas, P.; Loppinet, B.; Rakitzis, T. P. *J. Chem. Phys.* **2015**, *143*, 09B603_601.
- (21) Spiliotis, A. K.; Xygkis, M.; Klironomou, E.; Kardamaki, E.; Boulogiannis, G. K.; Katsoprinakis, G. E.; Sofikitis, D.; Rakitzis, T. P. *Chemical Physics Letters* **2020**, *747*, 137345.
- (22) Spiliotis, A. K.; Xygkis, M.; Klironomou, E.; Kardamaki, E.; Boulogiannis, G. K.; Katsoprinakis, G. E.; Sofikitis, D.; Rakitzis, T. P. *Laser Phys.* **2020**, *30*, 075602.
- (23) Visschers, J. C.; Tretiak, O.; Budker, D.; Bougas, L. *J. Chem. Phys.* **2020**, *152*, 164202.
- (24) Budker, D.; Gawlik, W.; Kimball, D. F.; Rochester, S. M.; Yashchuk, V. V.; Weis, A. *Reviews of modern physics* **2002**, *74*, 1153.
- (25) Bougas, L. *Cavity-enhanced polarimetry: applications in atomic parity violation and molecular chirality*. PhD Thesis, University of Crete, **2014**.
- (26) Ciaffoni, L.; Couper, J.; Hancock, G.; Peverall, R.; Robbins, P. A.; Ritchie, G. A. D. *Opt. Express, OE* **2014**, *22*, 17030-17038.
- (27) Manfred, K. M.; Kirkbride, J. M. R.; Ciaffoni, L.; Peverall, R.; Ritchie, G. A. D. *Opt. Lett., OL* **2014**, *39*, 6811-6814.
- (28) Pinto, T. H. P.; Kirkbride, J. M. R.; Ritchie, G. A. D. *Opt. Lett., OL* **2018**, *43*, 1931-1934.
- (29) Wiberg, K. B.; Wang, Y.-g.; Murphy, M. J.; Vaccaro, P. H. *J. Phys. Chem. A* **2004**, *108*, 5559-5563.
- (30) Lahiri, P.; Wiberg, K. B.; Vaccaro, P. H. *J. Phys. Chem. A* **2013**, *117*, 12382-12400.
- (31) Mason, M. G.; Schnepf, O. *J. Chem. Phys.* **1973**, *59*, 1092-1098.
- (32) Drakl, A. F.; Mason, S. F. *Tetrahedron* **1977**, *33*, 937-949.
- (33) Hawkins, J. E.; Armstrong, G. T. *J. Am. Chem. Soc.* **1954**, *76*, 3756-3758.
- (34) Fraser, D. G.; Fitz, D.; Jakschitz, T.; Rode, B. M. *Phys. Chem. Chem. Phys.* **2010**, *13*, 831-838.
- (35) Erastova, V.; Degiacomi, M. T.; G. Fraser, D.; Greenwell, H. C. *Nature Communications* **2017**, *8*, 2033.

